

Influence of Lattice Defects on *Trans*-Oligoene Substructure Formation in Graphene

Fabian Grote^[a] and Siegfried Eigler^{*[a]}

The photochemical reaction of iodine and graphene induces strong new Raman modes due to the formation of *trans*-oligoene substructures in graphene domains. This unique reactivity was demonstrated before on defect-free graphene, however leaving the influence of e.g. carbon vacancies, unexplored. Here, we investigate the photochemical reaction applied on graphene with varying average distances of lattice defects and statistically analyze the characteristic Raman modes which develop with the iodination reaction. We show that the iodination reaction does not lead to Raman-active defects and

thus, the newly formed *trans*-oligoene substructures do not contribute to the D-mode of graphene. A statistical analysis reveals the correlation between the average distance of lattice defects and the intensity of the ν_1 -mode. For defective graphene with average defect distances below ~ 1 nm no new Raman modes evolve, which is the lower limit of the substructure size probed at 532 nm and explains why this observation was not possible before using common graphene oxide as graphene source.

Introduction

The regioselective functionalization of graphene modifies its electronic structure by periodic variations on the nanometer scale within the graphene lattice.^[1] To date, examples of reactions generating defined substructures within the material are rare due to a lack of functionalization strategies with strong regioselectivity.^[2] Moiré superlattices of graphene and its metal substrate have been used to guide the reactivity in periodical patterns.^[3] Similar to the patterning on the microscopic scale, masks of supramolecular assemblies can be used to introduce periodic structures.^[4]

In our recent report, the evolution of *trans*-oligoene substructures induced by a photochemical iodination reaction applied on defect-free graphene was observed.^[5] However, previous reports using defective graphene, e.g. reduced graphene oxide did not display specific Raman modes, that would suggest a reaction with iodine.^[6] Thus, the substructure formation seems to be strongly influenced and limited by the presence of lattice defects. Generally, lattice defects strongly influence the electronic properties and determine the Raman scattering properties of graphene.^[7] Accordingly, vacancy defects can activate surrounding unsaturated carbon bonds and thus guide the reactivity of radical addition reactions, a process, which can be followed by Raman spectroscopy.^[8]

Consequently, the introduced functional groups majorly accumulate around defect sites, while large areas between them remain graphene-like. In addition, lattice defects act as scattering sites for phonons and therefore activate the D-peak in Raman spectra, which is used to quantify the distance of defects.^[9] Statistical Raman spectroscopy can be used to assess the quality of graphene^[10] and follow functionalization reactions with μm -scale spatial resolution.^[11] A precise relation between the Raman modes and the distance of defects was developed by Lucchese and Cançado^[9a] (Equation 1, Table S2) that empirically describes the relation of the ratio between the intensity of the D-mode (I_D) and the G-mode (I_G) and the average distance of defects in graphene.

$$\frac{I_D}{I_G} = C_A \frac{(r_A^2 - r_S^2)}{(r_A^2 - 2r_S^2)} \left[e^{-\frac{\pi r_A^2}{L_D^2}} - e^{-\frac{\pi(r_A^2 - r_S^2)}{L_D^2}} \right] \quad (1)$$

Here, L_D is the distance of defects in nm, C_A is an empirically derived parameter that depends on the laser energy used (2.33 eV, 532 nm in this work). The radius of the activated area (r_A) and the radius of the structurally disordered region (r_S) describe the contributions of these areas around the defects. This model was derived for graphene bombarded with Ar^+ ions and its applicability was also shown for other defective graphene materials proving its general applicability.^[10b,12]

Since *trans*-oligoene modes can be generated in defect-free graphene, but are not yet reported in reduced graphene oxide, statistical correlations between the *trans*-oligoene Raman modes, see Figure 1, and the distance of lattice defects may provide structural information of the novel substructures. Thus, we studied the extend of *trans*-oligoene substructure formation induced by the iodination reaction of different graphene samples with L_D -values ranging from no detectable defects down to below 1 nm. We show that the characteristic Raman modes emerge in defective graphene under similar reaction conditions reported for defect-free graphene. We further show

[a] M.Sc. F. Grote, Prof. Dr. S. Eigler
Institut für Chemie und Biochemie
Freie Universität Berlin
Altensteinstraße 23a, 14195 Berlin, Germany
E-mail: siegfried.eigler@fu-berlin.de

Supporting information for this article is available on the WWW under <https://doi.org/10.1002/chem.202401031>

© 2024 The Authors. Chemistry - A European Journal published by Wiley-VCH GmbH. This is an open access article under the terms of the Creative Commons Attribution License, which permits use, distribution and reproduction in any medium, provided the original work is properly cited.

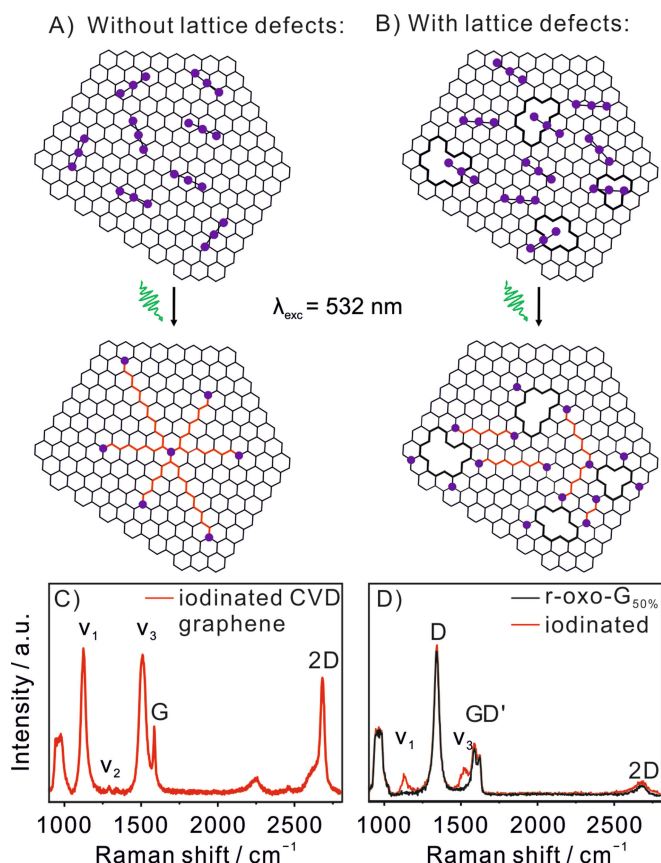


Figure 1. Schematic illustration of the functionalization process: Graphene is doped with polyiodides (purple) and is subsequently irradiated by laser light ($\lambda_{\text{exc}} = 532 \text{ nm}$) to generate iodine radicals that induce *trans*-oligoene substructures (red). A) In graphene without defects the length of the substructures is only limited by the delocalization of the π -radical. B) Radical addition reactions occur around defects that also limit the length of the substructures. C) Raman spectrum of iodinated CVD graphene without defects. Strong v_1 and v_3 -modes emerge and the v_2 -mode can be observed but no D-mode. D) Raman spectra of *r*-oxo- $G_{50\%}$ with $L_D \sim 2 \text{ nm}$ before (black) and after (red) iodination reaction. The v_1 and v_3 modes form while no significant change of the graphene modes is observed.

that no Raman-active defects are introduced by the reaction and hence the formation of *trans*-oligoene substructures can be followed. With Statistical Raman spectroscopy (SRS) we reveal a correlation between the distance of defects and the intensity of the *trans*-oligoene Raman modes. The characteristic modes do not appear at defect distances below about 1 nm, which therefore is the lower limit of *trans*-oligoene substructure length probed under the given conditions.

Results and Discussion

To investigate the influence of lattice defects on *trans*-oligoene chain formation, we iodinated different graphene derivatives on 300 nm SiO_2/Si substrate with various distances of lattice defects. Graphene with a heterogeneous quality was prepared by chemical vapor deposition (CVD) that cover the full range of defects in the Raman-sensitive range. Furthermore, we wet-chemically prepared oxo-graphene with defined distances of

defects depending on the oxidation conditions. Purified oxo-graphene was transferred onto SiO_2/Si substrate by drop-casting and reduced with hot vapors of hydrogen iodide and trifluoroacetic acid, as reported earlier.^[13] Depending on the oxo-functionalized graphene derivative, two kinds of graphene were prepared. The graphene derivative *r*-oxo- $G_{50\%}$ (the subscript indicates the degree of functionalization of oxo-graphene before reduction and the prefix “*r*” indicates that it was reduced to yield graphene) with $I_D/I_G = 2.6$ relates to $L_D \sim 2 \text{ nm}$ (Figure S1A) and *r*-oxo- $G_{4\%}$ with $I_D/I_G = 3.1$ relates to $L_D \sim 6 \text{ nm}$ (Figure S1B), according to Equation 1. The atomic structures of those materials have been visualized by ac-TEM before.^[14] A methanolic iodine solution (20 mM, 10 μL) was deposited onto the sample for the photochemical reaction and after complete evaporation of the solvent the sample was irradiated by the Raman laser (532 nm, 0.1 s irradiation time, 10 accumulations, Figure 1A and B). To exclude laser induced side reactions the experiments were tested without iodine as well, but no significant changes were observed.

Further on, we investigated whether Raman-active defects are introduced by the iodination reaction. No D-peak formation was observed for graphene without defects, as depicted in Figure 1C. Next, we used reduced oxo-graphene with an average defect distance of about 2 nm, for which Raman spectroscopy is most sensitive on changes in the distance of defects by monitoring the I_D/I_G ratio (Figure 1D). Despite the significant density of defects, v_1 and v_3 modes emerge in the Raman spectra, however with a ~ 10 times decreased intensity compared to defect-free graphene. Interestingly, the I_D/I_G ratio did not change within the limits of the reference experiment (Table S1) showing that any defects introduced by the iodination reaction must be either Raman silent or below the detection limit.

The covalent addition of substituents without significant D-mode introduction in graphene has been reported earlier, e.g. for chlorination and azidation reactions.^[15] It has also been reported for the addition of nitrenes on carbon nanotubes, where re-aromatization after the addition reaction is proposed as explanation.^[16] We expect that for halogen reactions zigzag edges are formed between the *trans*-oligoene chains and the graphene domains, which are known as Raman silent.^[17] Consequently, this allows us to correlate the Raman modes of graphene with lattice defects and the *trans*-oligoene signals. Thus, we used the heterogeneous CVD graphene to ensure same experimental conditions (laser power, amount of iodine) for all data points of the Raman maps, as displayed in Figure 2A. 528 spectra were collected and filtered to exclude substrate and adlayer spectra prior to analysis yielding a data set of 256 monolayer spectra of heterogeneous CVD graphene. Those spectra were fitted using Lorentzian functions (Figure S2A). The area of the D-mode (A_D) was used as a measure for defects since it steadily increases with increasing density of defects and is also related to the distance of defects. Vecera *et al.* reported that A_D increases exponentially with the introduction of defects, which is also observed in our data set (Figure S2B).^[18] This strong sensitivity allows the detection of minor changes within the graphene lattice.

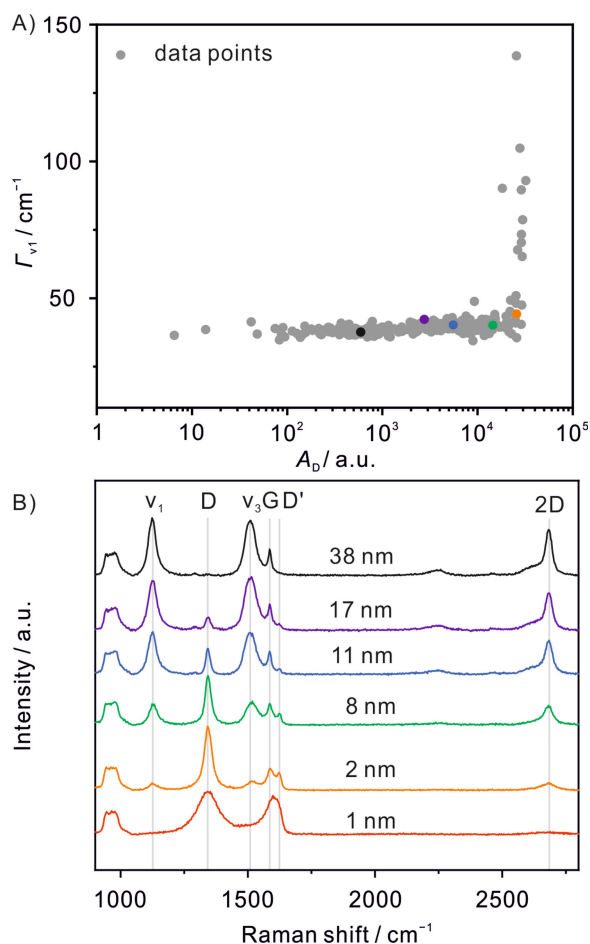


Figure 2. A) Scatter plot of Γ_{v_1} against A_D of heterogenous CVD graphene. The coloured dots are the spectra shown in B. B) Raman spectra of iodinated CVD graphene with increasing defect densities ($\lambda_{\text{exc}} = 532 \text{ nm}$). The important Raman modes are marked with grey lines.

Plotting the full-width at half-maximum (Γ_{v_1} , $\sim 38 \text{ cm}^{-1}$, Figure 2A) and the peak position (χ_{v_1} , $\sim 1125 \text{ cm}^{-1}$) against A_D shows that these properties do not significantly vary over a large range of defect distances (Figure S3A and B). After irradiation, we generally observe that the intensity of the v_1 - and v_3 - modes are lower when the D- and D'-mode are stronger (Figure 2B). At $L_D < 2 \text{ nm}$ the decreasing intensity of the v_1 -mode and the simultaneous increase of the D-mode make proper fitting of peaks challenging (spectra marked with an asterisk in Figure 3A) due to the overlap of D- and v_1 -peak (Figure S4) and I_{v_1} was approximated here. Plotting A_{v_1} and I_{v_1} against A_D shows that they are stable over three orders of magnitude before they drop at $A_D \sim 10,000$ when plotted on a double logarithmic scale (Figure S3C and D) and increase again at high defect densities due to the increasing overlap of the D-mode in the area (Figure S4). Since I_{v_1} decreases as the number of defects increases, we assume that it is related to the number of *trans*-oligoene substructures with a matching bandgap in the probed area by the 532 nm laser.

The measured data were fitted by an exponential decay function, as described by Equation 2 where I_0 is the intensity of v_1 without defects and a is an empirical parameter (Figure 3A).

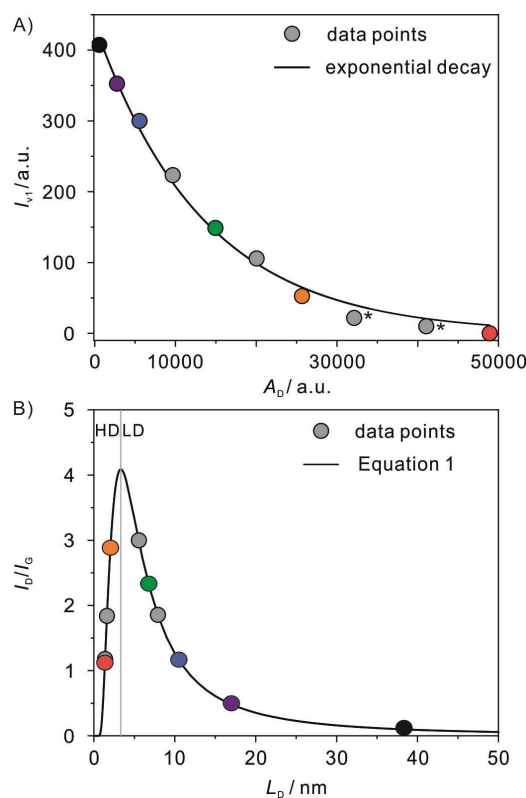


Figure 3. A) Plot of I_{v_1} over A_D including the spectra shown in A. The data are in good agreement with an exponential decay fit (Equation 2). For spectra marked with an asterisk v_1 and v_3 could not be fitted anymore and I_{v_1} was estimated (Figure S3). B) I_{v_1}/I_0 ratios plotted against L_D ; the solid line follows Equation 1. HD: high defect regime, LD: low defect regime. To distinguish between the HD and LD, I_{2D} (50 cm^{-1}) was used.

$$I_{v_1}(A_D) = I_0 e^{-\frac{A_D}{a}} \quad (2)$$

The observed correlation demonstrates the dependance of lattice defects in graphene and the formation of *trans*-oligoene substructures upon iodination reaction. The fitted parameters are summarized in Table S2. The fitting function covers the full range of defects and reveals a continuous correlation in the low- and high defect regimes (Figure 3B). For highly defective graphene with $L_D < 1 \text{ nm}$ the material structure significantly differs from intact graphene since defective graphene is polydisperse with carbon domains, which even no longer bear hexagonal carbon lattices and thus contain next to point-like defects, large holes, and also amorphous carbon domains.^[19] Therefore, graphene with such high defect density is not suited for the formation *trans*-oligoene substructures. This observation can explain the absence of characteristic signals in defect-rich reduced graphene oxide, since the absence of sufficiently large graphene domains and the exponential increase of the graphene Raman modes would prevent the detection of *trans*-oligoene substructures.

Due to the resonance Raman effect only *trans*-oligoene chains with a bandgap close to the laser energy (2.33 eV) can be detected.^[20] The observed signals are in good agreement with those of *tbu*-capped *trans*-oligoene molecules (Figure S5) reported by Schaffer *et al.*^[21] containing around eleven double

bonds (bandgap: 2.35 eV, $\nu_1=1125.1\text{ cm}^{-1}$, $\nu_3=1514\text{ cm}^{-1}$). Such a carbon chain would have a length of $\sim 2.6\text{ nm}$, larger than the observed limit in our Raman spectra but on the same order of magnitude. Shorter substructures with a larger bandgap may also be present within the graphene domains (Figure 4) but are difficult to probe due to the reported defunctionalization at higher excitation energies.^[5]

In graphene without defects the maximum chain length of *trans*-oligoene substructures is only limited by the extent of the π -radical delocalization within the graphene lattice. In defective graphene the reactivity towards iodine radicals is increased on the one hand, on the other hand defects limit the extension of π -radicals and therefore, the achievable *trans*-oligoene chain length is limited. In defective CVD graphene typical lattice defects are rearranged carbons, such as Stone-Wales defects and extended line defects.^[7] In addition, the carbon lattice may be ruptured by the transfer process causing additional lattice defects. Reduced oxo-graphene consists of graphene with point defects and larger holes that are introduced by overoxidation of the graphene lattice during the functionalization process. From previous aberration corrected transmission electron microscopy (ac-TEM) studies the atomic structure of thermally annealed oxoG_{4%} was visualized and consists of graphene domains with few point-defects and holes due to the disproportionation of oxygen containing groups, resulting in L_D values of about 5–10 nm.^[22]

Even for graphene with more defects, e.g. obtained from thermal annealing of oxo-G_{50%}, at 300 °C highly intact graphene domains with diameters of $\sim 5\text{ nm}$ have been observed by ac-

TEM that would still allow *trans*-oligoene substructure formation, although most other graphene domains have diameters of about 1 nm.^[19] This demonstrates the heterogeneity of defective graphene and the limitation of the model of statistically distributed defects within an otherwise intact graphene lattice. Thus, the inhomogeneity of materials can explain the emergence of *trans*-oligoene Raman signals at defect distances smaller than the length of the probed substructures. Due to the small number of such domains the observed signal is minor, since the major amount of present carbon results in larger signals (see Supplementary Note 5). The constant I_{ν_1} and $x_{C_{\nu_1}}$ suggest a narrow distribution of *trans*-oligoene substructures (Figure S2), as expected by resonance Raman spectroscopy.^[23] The strong decrease of I_{ν_1} is in good agreement with the necessity of intact graphene domains for *trans*-oligoene substructure formation, as evident in Figure 4: Iodine radicals add to defect-activated carbon bonds close to lattice defects and form *trans*-oligoene substructures by isolation of double bonds between the sp^3 -defects. Thus, the number and length of the substructures are limited by the size of the intact graphene domains, which explains the disappearance of the *trans*-oligoene Raman modes in the high defect regime.

Conclusions

Trans-oligoene substructure formation can be induced in graphene with lattice defects via photochemical iodination reaction and characteristic Raman modes are observed. No significant change of the D-mode intensity is detected in the most Raman-sensitive defect regime with defect distances around 2–3 nm, suggesting that newly formed defects by the iodination reaction are Raman silent or below the detection limit. For addition reactions to graphene, the reaction is mostly followed by D-mode formation and therefore, no study was possible investigating reactions on graphene without affecting the D-mode. Since the formation of *trans*-oligoene substructures does not affect the D-mode of graphene, the iodination reaction could be monitored by Raman spectroscopy as a function of defect density. Statistical Raman analysis of graphene samples with varying defect distances reveals the correlation between I_{ν_1} and the number of lattice defects, underscoring the strong dependence of *trans*-oligoene substructure formation on structural defects within the graphene lattice. At defect distances below $\sim 1\text{ nm}$ no *trans*-oligoene Raman modes are observed, indicating that the size of the remaining intact graphene domains becomes too small for their formation and ability for probing by 532 nm laser excitation. Our observations may be exploited in the future to drive regiochemical functionalization strategies of graphene-type materials, leading to periodically functionalized materials suitable for various fields of research.

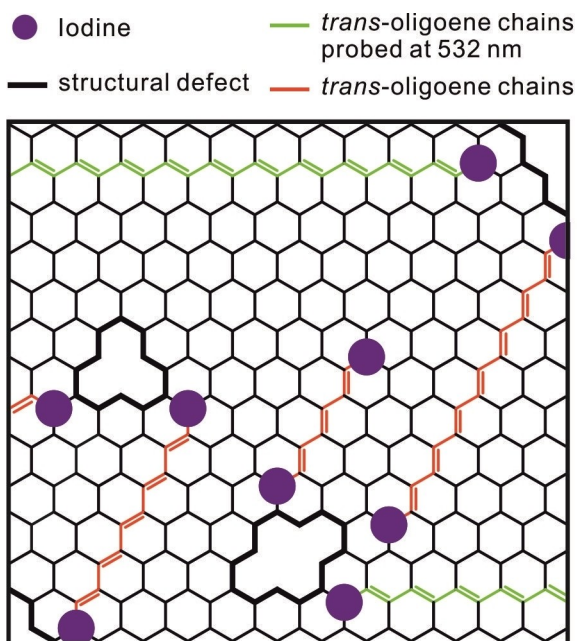


Figure 4. Schematic illustration of the proposed *trans*-oligoene substructures in defective graphene. Structural defects are starting points of substructure formation due to increased reactivity and limit the size of intact graphene domains. Substructures with a bandgap close to the laser energy (2.33 eV) are probed (green) while shorter ones with a larger bandgap (red) do not contribute significantly to the resonance Raman signal. Double bonds of graphene have been omitted for clarity.

Experimental Section

Materials and Methods

Methanol used for sample preparation was distilled in a solvent circulation apparatus to remove any impurities before use. Iodine was purchased from TCI and used as received. Graphite type 3061 was obtained from Asbury Carbon Mills and all other materials were purchased from Sigma-Aldrich and used as received. Si wafers with a 300 nm thick SiO₂ layer were purchased from Fraunhofer Institut für Integrierte Systeme und Bauelementetechnologie IISB in Erlangen. Thermal annealing of samples in vacuum was made using a Nabertherm 30–3,000 °C oven.

Raman Spectroscopy

Statistical Raman spectroscopic characterization was carried out on a Horiba Jobin Yvon XploRA™ PLUS spectrometer equipped with a confocal microscope and an automated XYZ table. Spectra were recorded with a green laser (532 nm, 2.33 eV) combined with a 100x objective resulting in a spot size of about 700 nm and 1,200 grooves mm⁻¹ grating was used. The Raman shift was calibrated to the Si peak before measurement.

Raman data were analyzed using the Origin 2019b software and signals were fitted using single Lorentzian functions. Baseline corrections were directly made in the LabSpec6 software of the instrument and spikes were removed prior to data analysis. Statistical Raman data were analyzed using a Python script. The ν₁-, D- and 2D-modes were fitted using single Lorentzian functions, while a triple Lorentzian function was used between 1450–1650 cm⁻¹ to fit the ν₃-, G- and D'-modes.

Preparation of CVD Graphene

Graphene was prepared by chemical vapor deposition on copper foil using the envelope method.^[24] After annealing of the copper envelope for 1 h (1035 °C, 10 sccm H₂, 5 sccm Ar) a flow of methane (5 sccm) was added to the mixture for 10 min growth time. Then, the sample was rapidly cooled down to rt. Controlling growth time is critical if a heterogenous quality of graphene is desired.^[25] The exact reaction time depends however on the setup. Arbitrary pieces of graphene were transferred onto substrates by wet-transfer method.

Preparation of oxo-G_{4%}

High-quality oxo-functionalized graphene was prepared by our earlier reported method.^[14] The oxo-graphite crystals were repeatedly washed by centrifugation and decanting of excess aqueous solution until a neutral pH was reached. The oxo-graphite crystals were freeze-dried in a lyophilizer to remove remaining water. High quality samples were prepared by tape exfoliation using the Scotch tape method and directly transferred onto SiO₂/Si substrates. After reduction, the samples were annealed in vacuum ($T=300\text{ }^{\circ}\text{C}$, $p=1\times 10^{-3}\text{ mbar}$, $t=2\text{ h}$) to remove any remaining residues.

Preparation of oxo-G_{50%}

Oxo-graphene with a degree of functionalization around 50% was prepared by our controlled synthesis approach, reported earlier.^[13]

Reduction of oxo-G with HI/TFA

Oxo-graphene was reduced using a mixture of HI and TFA according to our method published elsewhere.^[26] Samples were reduced in the vapors of HI and TFA at 80 °C for 5 min. The wafers were placed on the hotplate for 5 min to remove any remaining reducing agents.

Photochemical Iodination Reaction

A solution of iodine in methanol (20 mM, 10 μL) was applied to the sample on the wafer. After complete evaporation of the solvent the sample was irradiated. Measurements of Raman spectra and the patterning experiments were performed at 3 mW laser power. Spectra were measured with an acquisition time of 0.1 s. The light dosage was controlled by the exposure time. For functionalization, 10 accumulations per spot were used with a total irradiation time of 1 s.

Acknowledgements

SE and FG gratefully acknowledge funding from Deutsche Forschungsgemeinschaft (DFG, German Research Foundation, Project No. 392444269). Open Access funding enabled and organized by Projekt DEAL.

Conflict of Interests

The authors declare no conflict of interest.

Keywords: defects · graphene · iodine · Raman spectroscopy · substructures

- [1] I. Piquero-Zulaica, J. Lobo-Checa, Z. M. A. El-Fattah, J. E. Ortega, F. Klappenberger, W. Auwärter, J. V. Barth, *Rev. Mod. Phys.* **2022**, *94*.
- [2] T. Wei, F. Hauke, A. Hirsch, *Adv. Mater.* **2021**, *33*, e2104060.
- [3] J. J. Navarro, S. Leret, F. Calleja, D. Stradi, A. Black, R. Bernardo-Gavito, M. Garnica, D. Granados, A. L. Vazquez de Parga, E. M. Perez, R. Miranda, *Nano Lett.* **2016**, *16*, 355.
- [4] a) M. Guo, Z. Qu, F. Min, Z. Li, Y. Qiao, Y. Song, *InfoMat* **2022**, *4*; b) M. Yu, C. Chen, Q. Liu, C. Mattioli, H. Sang, G. Shi, W. Huang, K. Shen, Z. Li, P. Ding, P. Guan, S. Wang, Y. Sun, J. Hu, A. Gourdon, L. Kantorovich, F. Besenbacher, M. Chen, F. Song, F. Rosei, *Nat. Chem.* **2020**, *12*, 1035.
- [5] F. Grote, B. I. Weintrub, M. Kressler, Q. Cao, C. E. Halbig, P. Kusch, K. I. Bolotin, S. Eigler, *Small* **2024**, e2311987.
- [6] a) P. Šimek, K. Klímová, D. Sedmidubský, O. Jankovský, M. Pumera, Z. Sofer, *Nanoscale* **2015**, *7*, 261; b) A. Wang, S. Bok, C. J. Mathai, K. Gangopadhyay, J. McFarland, M. R. Maschmann, S. Gangopadhyay, *Nano Futur.* **2020**, *4*; c) J. Chen, M. W. Xu, J. Wu, C. M. Li, *Nanoscale* **2018**, *10*, 9115; d) M. S. Mirshekarloo, M. C. D. Cooray, P. Jovanović, C. D. Easton, F. Wu, T. D. Gamot, M. J. Abedin, M. R. Yuce, M. Shaibani, M. Majumder, *Batteries & Supercaps* **2021**, *4*, 1175.
- [7] M. D. Bhatt, H. Kim, G. Kim, *RSC Adv.* **2022**, *12*, 21520.
- [8] a) C. E. Halbig, R. Lasch, J. Krüll, A. S. Pirzer, Z. Wang, J. N. Kirchoff, K. I. Bolotin, M. R. Heinrich, S. Eigler, *Angew. Chem. Int. Ed.* **2019**, *58*, 3599; b) Y. Wang, F. Grote, Q. Cao, S. Eigler, *J. Phys. Chem. Lett.* **2021**, *12*, 10009.
- [9] a) M. M. Lucchese, F. Stavale, E. H. M. Ferreira, C. Vilani, M. V. O. Moutinho, R. B. Capaz, C. A. Achete, A. Jorio, *Carbon* **2010**, *48*, 1592; b) L. G. Cançado, A. Jorio, E. H. Ferreira, F. Stavale, C. A. Achete, R. B. Capaz, M. V. Moutinho, A. Lombardo, T. S. Kulmala, A. C. Ferrari, *Nano Lett.* **2011**, *11*, 3190.

- [10] a) S. J. Goldie, S. Bush, J. A. Cumming, K. S. Coleman, *ACS Appl. Nano Mater.* **2020**, *3*, 11229; b) S. Eigler, F. Hof, M. Enzelberger-Heim, S. Grimm, P. Müller, A. Hirsch, *J. Phys. Chem. C* **2014**, *118*, 7698; c) A. A. Graf, S. P. Ogilvie, H. J. Wood, C. J. Brown, M. Tripathi, A. A. K. King, A. B. Dalton, M. J. Large, *Chem. Mater.* **2020**, *32*, 6213.
- [11] J. M. Englert, P. Vecera, K. C. Knirsch, R. A. Schäfer, F. Hauke, A. Hirsch, *ACS Nano* **2013**, *7*, 5472.
- [12] S. Eigler, C. Dotzer, A. Hirsch, *Carbon* **2012**, *50*, 3666.
- [13] S. Eigler, *Chemistry* **2016**, *22*, 7012.
- [14] S. Eigler, *Chem. Commun.* **2015**, *51*, 3162.
- [15] a) G. Copetti, E. H. Nunes, G. K. Rolim, G. V. Soares, S. A. Correa, D. E. Weibel, C. Radtke, *J. Phys. Chem. C* **2018**, *122*, 16333; b) W. Li, Y. Li, K. Xu, *Nano Lett.* **2021**, *21*, 1150; c) X. Zhang, A. Hsu, H. Wang, Y. Song, J. Kong, M. S. Dresselhaus, T. Palacios, *ACS Nano* **2013**, *7*, 7262; d) W. Li, Y. Li, K. Xu, *Nano Lett.* **2020**, *20*, 534.
- [16] A. Setaro, M. Adeli, M. Glaeske, D. Przyrembel, T. Bisswanger, G. Gordeev, F. Maschietto, A. Faghani, B. Paulus, M. Weinelt, R. Arenal, R. Haag, S. Reich, *Nat. Commun.* **2017**, *8*, 14281.
- [17] C. Casiraghi, A. Hartschuh, H. Qian, S. Piskanec, C. Georgi, A. Fasoli, K. S. Novoselov, D. M. Basko, A. C. Ferrari, *Nano Lett.* **2009**, *9*, 1433.
- [18] P. Vecera, S. Eigler, M. Kolesnik-Gray, V. Krstic, A. Vierck, J. Maultzsch, R. A. Schäfer, F. Hauke, A. Hirsch, *Sci. Rep.* **2017**, *7*, 45165.
- [19] Z. Wang, Q. Yao, C. Neumann, F. Börrnert, J. Renner, U. Kaiser, A. Turchanin, H. J. W. Zandvliet, S. Eigler, *Angew. Chem. Int. Ed.* **2020**, *59*, 13657.
- [20] K. Furuya, A. Sakamoto, M. Tasumi, *J. Phys. Chem. A* **2023**, *127*, 5344.
- [21] H. E. Schaffer, R. R. Chance, R. J. Silbey, K. Knoll, R. R. Schrock, *J. Chem. Phys.* **1991**, *94*, 4161.
- [22] F. Grote, C. Gruber, F. Börrnert, U. Kaiser, S. Eigler, *Angew. Chem. Int. Ed.* **2017**, *56*, 9222.
- [23] H. Kuzmany, *Macromol. Symp.* **1990**, *37*, 81.
- [24] X. Li, C. W. Magnuson, A. Venugopal, R. M. Tromp, J. B. Hannon, E. M. Vogel, L. Colombo, R. S. Ruoff, *J. Am. Chem. Soc.* **2011**, *133*, 2816.
- [25] T. Niu, M. Zhou, J. Zhang, Y. Feng, W. Chen, *J. Am. Chem. Soc.* **2013**, *135*, 8409.
- [26] S. Eigler, S. Grimm, M. Enzelberger-Heim, P. Müller, A. Hirsch, *Chem. Commun.* **2013**, *49*, 7391.

Manuscript received: March 13, 2024

Accepted manuscript online: April 8, 2024

Version of record online: May 3, 2024